3D object recognition using fully intrinsic skeletal graphs

Djamila Aouada[a] and Hamid Krim[b]

North Carolina State University,
Electrical and Computer Engineering Department,
Raleigh, NC 27695, USA

ABSTRACT

In this paper, we propose a new topology extraction approach for 3D objects. We choose a normalized robust and simplified geodesic-based Morse function to define skeletal Reeb graphs of 3D objects. In addition to scale invariance, we ensure, by using a geodesic distance, the invariance of these graphs to all isometric transforms. In our Reeb graph construction procedure, we introduce important improvements and advantages over existing techniques. We define an efficient sampling rate based on the characteristic resolution intrinsic to each 3D object. Then, we provide a geometry preserving approach by replacing the traditional intervals of a Morse function by its exact level curves. Moreover, we take advantage of the resulting ordered adjacency matrices that describe our Reeb graphs, to introduce a new measure of similarity between the corresponding objects. Experimental results illustrate the computational simplicity and efficiency of the proposed technique for topological Reeb graphs' extraction. The experiments also show the robustness of this approach against noise and object remeshing.

Keywords: 3D object, topological modeling, Morse theory, Reeb graph, GGF.

1. INTRODUCTION

Thanks to the fast development of 3D data rendering and acquisition techniques, the applications related to 3D models (security, multimedia, biology, ...etc) have received, during the last decade, a great attention from both the scientific and the engineering communities. One of their most important objectives is to be able to simply represent 3D objects in order to efficiently achieve operations such as object classification, recognition and retrieval. Many approaches were recently defined to describe a 3D object. They are well summarized in [1] and .[2] In the present work, we represent objects through their topology ,[3] ,[4] ,[5] .[8] While extracting the topological features is our main goal, we also anticipate on a very probable need for an extension to a topology-geometry mixture that may arise from some applications such as recognition ,[6] [7] and [9]v. More specifically, we are interested in the work of Hilaga *et al.* [3] who introduce *Reeb* graphs for 3D objects using an approximation of an integrated geodesic *Morse* function ,[15],[13] .[14] Since a geodesic distance is involved, the 3D object representation becomes fully intrinsic to the surface of the object. However, this method remains fairly complex to compute as it requires a heavy preprocessing procedure to be applied on objects' triangulated meshes. Besides, it relies on an arbitrary choice for a parameter very important for the accuracy of the final topological graph. The parameter in question is the threshold delimiting patches around the so called base vertices. Hence, for our *Reeb* graph extraction, we use a more robust and simplified version of the integrated geodesic function. Indeed, we choose as our Morse function a different approximation first defined in [10] and referred to as *Global Geodesic Function GGF*. Furthermore, we directly relate the lowest accurate resolution * of an object, namely the *characteristic resolution*, to its meaningful curvatures and use this intrinsic information to define a sampling rule, analogous to the sampling rule for 3D objects. By so doing, we define the accurate resolution that ensures a correct approximation of the shape of a given 3D object. Thus, we no longer use the traditional solutions, often tricky and unprecise, for the choice of the sampling rate (either arbitrary/emperical choice or multi-resolutional sweeping of different sampling rates for every object). In ,[3] part of the operation of preprocessing the mesh is to subdivide the faces such that they fall exactly at a discrete level of the *Morse* function determined by

Further author information: (Please send correspondence to D. Aouada.)
[a]D. Aouada: E-mail: daouada@ncsu.edu, Telephone: 1 919 5157807;
[b]H. Krim.: E-mail: ahk@ncsu.edu, Telephone: 1 919 5132270
*Number of points approximating the surface of an object

Computational Imaging VI, edited by Charles A. Bouman, Eric L. Miller, Ilya Pollak,
Proc. of SPIE-IS&T Electronic Imaging, SPIE Vol. 6814, 681409, © 2008 SPIE-IS&T · 0277-786X/08/$18

the sampling rate. This obviously might eliminate one of the advantages of using a characteristic resolution. Therefore, we thought of a completely different procedure in determining the level sets of the *Morse* function. Instead of approximating a level set by an interval and thereby losing the inherent geometric information of an object, we choose to represent level sets of the *GGF* by their interpolated curves, *i.e.*, *iso-geodesic* curves, sitting at discrete values of the *GGF*. The remainder of the paper is organized as follows: In the next section, we start by giving a brief background review of *Morse* theory and *Reeb* graphs. Then, we give a summary of the method presented in [3] and highlight the advantages of using the *GGF*. In section 3, we present our procedure for *Reeb* graph extraction by defining our new key tools, *i.e.*, the sampling rule and the iso-geodesic curves. In Section 4, we present some experimental results and show the many advantages of the proposed *Reeb* graphs. Finally, we give our conclusions and perspectives in Section 5.

2. BACKGROUND

In this work, we view 3D objects as 2-dimensional smooth and compact surfaces $\mathcal{S}$ embedded in $\mathbb{R}^3$.

2.1 Morse theory and Reeb graphs

In order to extract the topological features of 3D objects, we make an extensive use of *Morse theory* .[15] *Morse theory* states that it is possible to define a particular smooth function f on a smooth surface $\mathcal{S}$ and track its critical points in order to study the topological changes on $\mathcal{S}$. Such a function f is called *Morse* function and is defined as follows:

DEFINITION 1. *A smooth function $f : \mathcal{S} \to \mathbb{R}$ on a smooth manifold $\mathcal{S}$ is called* Morse *if all of its critical points are non-degenerate.* A *Reeb* graph consists in defining the level sets of a defined *Morse* function. Mathematically, a *Reeb* graph may be defined as a quotient space $\mathcal{S}/\sim$, where the equivalence relation is given by $\mathbf{p} \sim \mathbf{q}$ if and only if $f(\mathbf{p}) = f(\mathbf{q})$ with $\mathbf{p}, \mathbf{q}$ being two points on $\mathcal{S}$ and belonging to the same connected component of $f^{-1}(f(\mathbf{p}))$. One of the simplest *Morse* function is the *height* function [16] that is usually used to illustrate the principle of *Reeb* graphs. The image of a point $\mathbf{p}$ on $\mathcal{S}$ via the height function is reduced to its z coordinate. The rotation invariance of 3D object descriptors is one of the properties that are required by the majority of 3D object applications. It is obvious that *Reeb* graphs using a height function do not verify this property. More generally, it is important to note that the properties of the chosen *Morse* function directly influence the properties of the final *Reeb* graph. Therefore, in order to ensure an intrinsic representation invariant to all isometric transforms, Hilaga *et al.* define their *Morse* function at a point $\mathbf{v}$ on $\mathcal{S}$ as the integral of the geodesic distance $\mathrm{d}(\mathbf{v}, \mathbf{p})$ from $\mathbf{v}$ to all other points $\mathbf{p}$ on $\mathcal{S}$.

$$f(\mathbf{v}) = \int_{\mathbf{p} \in \mathbf{S}} \mathbf{d}(\mathbf{v}, \mathbf{p}) \mathbf{d}\mathcal{S}. \tag{1}$$

Their discrete approximation of (1), that we herein call first approximation $f_{appr1}(\cdot)$, is as follows:

$$f_{appr1}(\mathbf{v}) = \sum_i \mathbf{d}(\mathbf{v}, \mathbf{b}_i) \cdot \mathbf{area}(\mathbf{b}_i), \tag{2}$$

where $\{\mathbf{b}_i\}_{i=\mathbf{0},\mathbf{1},\ldots}$ is a finite countable set of base vertices scattered on $\mathcal{S}$ and $\mathbf{area}(\mathbf{b}_i)$ is the area that $\mathbf{b}_i$ occupies, such that, $\sum_i \mathbf{area}(\mathbf{b}_i) \approx \mathbf{area}(\mathcal{S})$. Also, for an accurate result, Hilaga *et al.* emphasize on the need for a mesh preparation through two operations: generation of short-cut edges based on a manually chosen threshold and a subdivision of the mesh.

2.2 Global Geodesic Function *GGF*

Let's consider the object "droplet" of Figure 1. and compute its integrated geodesic function. Because of the perfect symmetry of this 3D shape with respect to the z axis, one should expect the function f defined in (1) to have all its level sets exactly parallel to the xy plane , *i.e.*, horizontally constant. However, we find that failure in achieving an appropriate prepossessing of the mesh may drastically affect the distribution of f_{appr1}, the first approximation of f as defined in (2). On Figure 1, we see that the colors on **a** are not uniform as they should be and are on **c**, hence our motivation in using a different approximation of f as our *Morse* function while keeping similar attractive properties, that is a full invariance to isometric transformations, and further improving the

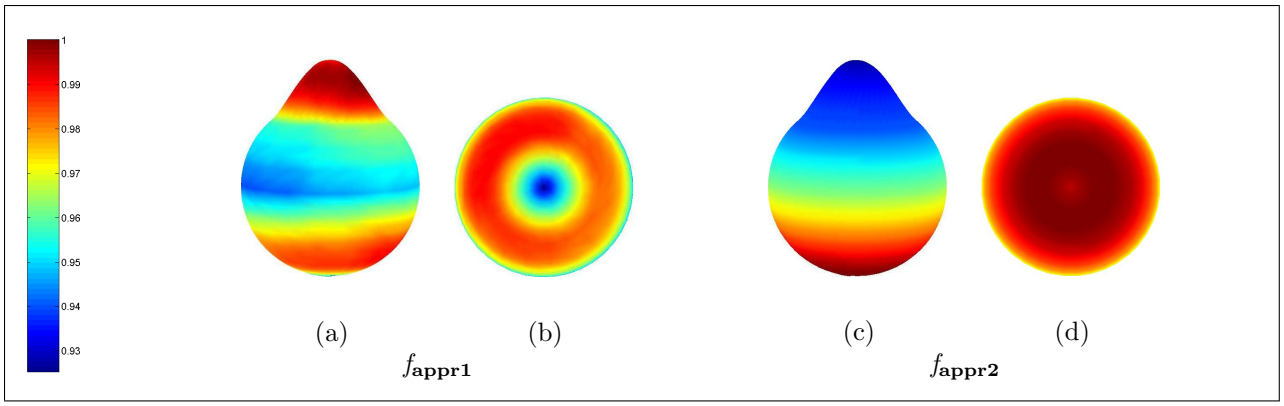

Figure 1. Comparison of the two approximation of the integrated geodesic *Morse* function. **a** and **b** are, respectively, the front and bottom views of the distribution of $f_{\mathbf{appr1}}(\cdot)$ on the object "droplet". **c** and **d** are, respectively, the front and bottom views of the distribution of $f_{\mathbf{appr2}}(\cdot)$ on the object "droplet".(Best visualized in color)

robustness to surface meshing and noise. Thus, we use the approximation $f_{appr2}(\cdot)$ defined by Aouada *et al.* and referred to as *GGF*.

$$f_{appr2}(\mathbf{v}) = \frac{\sum_{\mathbf{p}\in\mathcal{S}} \mathbf{d}(\mathbf{v},\mathbf{p})}{\max_{\mathbf{q}\in\mathcal{S}} \left(\sum_{\mathbf{p}\in\mathcal{S}} \mathbf{d}(\mathbf{q},\mathbf{p})\right)}. \tag{3}$$

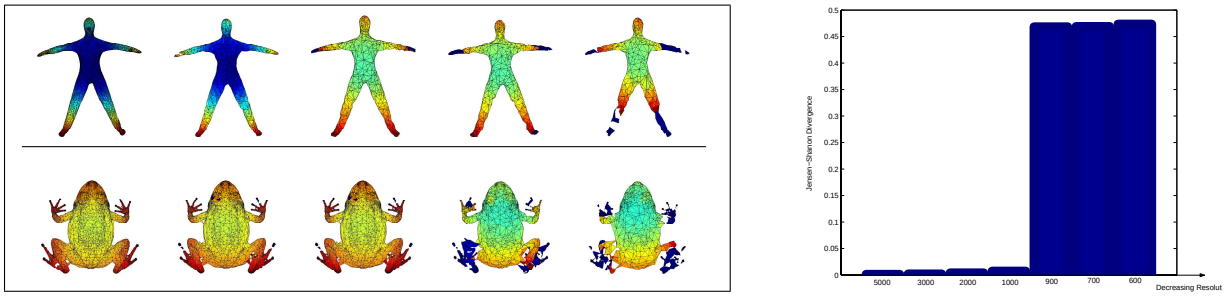

(a) (b)

Figure 2. Illustration of the characteristic resolution extraction (Best visualized in color).

As explained in ,[10] the *GGF* is robust against surface remeshing. Moreover, it is efficiently computed if used at the *characteristic resolution* $\mathcal{R}$ of a surface $\mathcal{S}$. The parameter $\mathcal{R}$ is a feature parameter assigned to a surface $\mathcal{S}$ approximated by a mesh. $\mathcal{R}$ is the minimal number of points that correctly represent the shape of $\mathcal{S}$. We experimentally verify that a uniform subdivision of a mesh preserves a near invariance of the histogram of the *GGF* over the set of accurate resolutions. This invariance is abruptly lost as the number of vertices becomes insufficient. Figure 2. illustrates the effect of a progressive reduction of the resolution for different models starting from the best representation. The best representation or best *GGF* is, of course, the one that corresponds to the highest resolution. We subsequently compare the distribution of the best *GGF* computed at the resolution R_0 to those obtained by progressively decreasing the resolutions. To this end, we use the square root of *Jensen-Shannon Divergence JSD* as a distance function between two distributions ,[12] .[?] The *JSD* between two *probability mass functions pmf*s P and Q is defined as follows:

$$JSD(P,Q) = H\left(\frac{P+Q}{2}\right) - \frac{H(P)+H(Q)}{2}, \tag{4}$$

where H is the *Shannon entropy* defined for any *pmf* P by $H(P) = -\sum_{i=1}^{L} P(i)\log P(i)$, with $P(i)$, $i = 1,\ldots,L$, being the elements of the discrete *pdf* vector P of length L. Considering K different resolutions, $R_0 > R_1 >$

$\ldots > R_{K-1}$, of the object of interest, and their K corresponding pmfs P_{R_i}, $i = 0, 1, \ldots, K-1$, we define:

$$\zeta(R_i) = \begin{array}{c} JSD(P_{R_0}, P_{R_i}) + JSD(P_{R_0}, P_{R_{i+1}}) - \\ 2\sqrt{JSD(P_{R_0}, P_{R_i}) \cdot JSD(P_{R_0}, P_{R_{i+1}})}. \end{array} \tag{5}$$

The characteristic resolution is then:

$$\mathcal{R} = \arg \max_{i=1,\ldots,K-1} \left(\zeta(R_i)\right). \tag{6}$$

$\mathcal{R}$ is a feature that is directly related to the curvature of a shape. As we reduce $\mathcal{R}$, we act on the original shape by smoothing it. This machinery is nothing but choosing a *tolerance* τ. *Tolerance* is the common name given for the maximal edge length between adjacent points on a surface $\mathcal{S}$.

3. REEB GRAPH EXTRACTION USING THE GGF

3.1 Efficient sampling

The sampling rate K is usually empirically chosen and the resulting sampling step is:

$$l = \frac{\max_{\mathbf{v}\in\mathcal{S}}\left(f(\mathbf{v})\right) - \min_{\mathbf{v}\in\mathcal{S}}\left(f(\mathbf{v})\right)}{K}. \tag{7}$$

A very redundant and important problem that is stressed when building *Reeb* graphs is how to solve this blind setting and define the effective sampling rate K that ensures the extraction of, and only of, the information needed to represent and reconstruct a given shape ,[3].[7] The use of curvature as a criterion is certainly the first thing that comes to one's mind. Indeed, if we think of planar shapes, we know that more points (vertices) are needed to represent high curvatures in opposition to straight line segments whose curvature is zero and for which the two extremal points are sufficient to represent and reconstruct the full shape. Our intuition may further suggest to take the highest curvature on the curve/surface to be the criterion. This would be the solution if the highest curvature happened to be a dominant feature on the whole shape. In many cases, this is not true. So instead of basing our choice on a local property, we rely on the global perception [Li] of shapes curvature. In 2.2, we saw how $\mathcal{R}$ is related to curvature. In fact, the raw data is reduced to its characteristic resolution $\mathcal{R}$ and every vertex becomes now of importance to obtain an accurate representation for $\mathcal{S}$. We recall that any topological transformation that happens on $\mathcal{S}$ and that we are to detect is translated on its one dimensional *Morse* function f. We, hence, take advantage of *Morse* theory again and base the sampling rule of a 3D object on the sampling of $f(\cdot)$ or of a functional of $f(\cdot)$. We view $f(\cdot)$ as a continuous random variable, or practically, $f_{appr2}(\cdot)$ as a discrete random variable X ($f_{appr2} \equiv X$), *s.t*, $X : \mathcal{V} \to \mathbb{R}$ is defined on the probability space $(\mathcal{V}, \mathcal{A}, P_R)$, where $\mathcal{V}$ is the set of $\mathcal{R}$ vertices on the triangle mesh $(\mathcal{V}, \mathcal{F})$ [†] approximating the surface $\mathcal{S}$. $\mathcal{A}$ is a $\sigma - Algebra$ composed of all the subsets of $\mathcal{V}$. Note that we interchangeably use $\mathcal{V}$ as the set or the matrix of vertices.

Just like in (7), we apply the sampling along the axis of variation of X. However, The sampling step l has to be efficient. To that end, we need to define the largest step l that will cause no breakdowns on the mesh $(\mathcal{V}, \mathcal{F})$. Let $\gamma_1 = {f^{-1}}_{appr2}\left(f_{appr2}(\mathbf{p})\right)$ and $\gamma_2 = {f^{-1}}_{appr2}\left(f_{appr2}(\mathbf{q})\right)$ be two distinct and consecutive connected components (that we will define as *iso-geodesic curves* in the next subsection). With a resolution $\mathcal{R}$ and a tolerance τ associated to it, the longest acceptable orthogonal geodesic distance between γ_1 and γ_2 is equal to τ. The remaining question is to find $l = |f_{appr2}(\mathbf{p}) - f_{\mathbf{appr2}}(\mathbf{q})| = |\lambda_{\mathbf{1}} - \lambda_{\mathbf{2}}|$. If $\mathbf{p}$ and $\mathbf{q}$ are connected then $\mathbf{d}(\mathbf{p}, \mathbf{q}) = \tau$, and we have for $\mathbf{v} \in \mathcal{V}$:

$$\mathbf{d}(\mathbf{p}, \mathbf{v}) > \mathbf{d}(\mathbf{p}, \mathbf{v}) \Longrightarrow \mathbf{d}(\mathbf{p}, \mathbf{v}) = \mathbf{d}(\mathbf{q}, \mathbf{v}) + \tau, \tag{8}$$

Similarly:

$$\mathbf{d}(\mathbf{p}, \mathbf{v}) < \mathbf{d}(\mathbf{p}, \mathbf{v}) \Longrightarrow \mathbf{d}(\mathbf{q}, \mathbf{v}) = \mathbf{d}(\mathbf{p}, \mathbf{v}) + \tau. \tag{9}$$

[†]A triangulated mesh is represented by the couple $(\mathcal{V}, \mathcal{F})$, where $\mathcal{V}$ is the matrix of vertices and $\mathcal{F}$ is the matrix of faces or triangles.

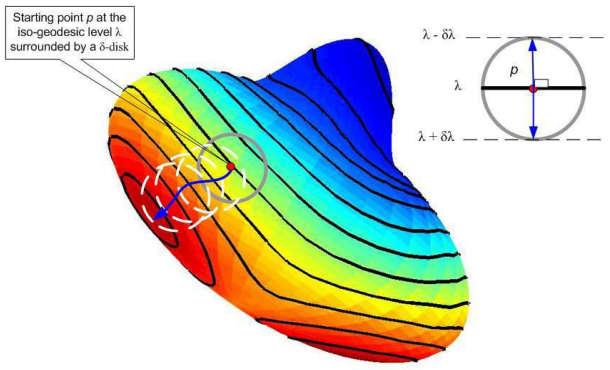

Figure 3. Illustration of iso-geodesic curves. The orthogonal curve is illustrated in thick blue. Patches are used for progressive projections.

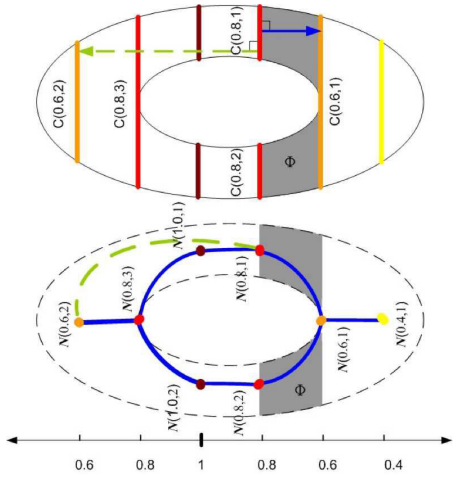

Figure 4. Nodes connectivity in 2-dimensions. Correct graph in blue. Paths in green are out of the section of interest Φ.

Therefore, if there are n elements from $\mathcal{V}$ verifying (8), then we find:

$$\lambda_1 - \lambda_2 = \frac{(\mathcal{R} - 2(n-1))}{\max_{\mathbf{v}\in\mathcal{V}} \sum_{\mathbf{w}\in\mathcal{V}} \mathbf{d}(\mathbf{v},\mathbf{w})} \cdot \tau. \tag{10}$$

We may also define an upper bound for l, independent of the variable n and equal to $\frac{(\mathcal{R}-2))}{\max_{\mathbf{v}\in\mathcal{V}} \sum_{\mathbf{w}\in\mathcal{V}} \mathbf{d}(\mathbf{v},\mathbf{w})} \cdot \tau$.

3.2 Iso-geodesic curves

As illustrated in ,[6] it is often necessary to add geometrical information to *Reeb* graphs to increase the power of discrimination of the final representation. In order not to refer to any mesh sub-sampling and not to loose the proposed advantages of using characteristic resolutions, we find the interpolated level sets at exact values of the *GGF*. We refer to the set of points sharing the same *GGF* value as an *iso-geodesic* set (Figure. 3).

For smooth and compact objects, an *iso-geodesic* set is proved to be the union of closed curves called *iso-geodesic* curves. The number of these distinct curves at the same geodesic level is the cardinality Car_i of the corresponding *iso-geodesic* set S_i. In the example of Figure 3, the illustrated *iso-geodesic* set corresponding to the value 0.8 of the *GGF* is of cardinality 2, that is it consists of two closed curves. In practice and on triangulated meshes, the extraction of an *iso-geodesic* set for a given level, say λ, consists first in finding all the faces that cover this set of curves. Each iso-geodesic curve is contained in a connected set of covering faces so that the resulting curve is ensured to be closed. Such a covering face whose vertices are $\mathbf{v_1}, \mathbf{v_2}$ and $\mathbf{v_3}$ with $f_{appr2}(\mathbf{v_1}) < f_{\mathbf{appr2}}(\mathbf{v_1}) < f_{\mathbf{appr2}}(\mathbf{v_1})$ has one of the following properties:

1. $\lambda \in [f_{appr2}(\mathbf{v_1}), f_{\mathbf{appr2}}(\mathbf{v_2})]$ or
2. $\lambda \in [f_{appr2}(\mathbf{v_2}), f_{\mathbf{appr2}}(\mathbf{v_3})]$

Two points $\mathbf{p_1}$ and $\mathbf{p_2}$ belonging to the approximated *iso-geodesic* set $\mathcal{S}_\lambda$ are defined on two edges of the covering face. If the property 1. is verified, then:

$$\overrightarrow{\mathbf{v_1 p_1}} = \frac{\lambda - f_{appr2}(\mathbf{v_1})}{f_{appr2}(\mathbf{v_3}) - f_{\mathbf{appr2}}(\mathbf{v_1})} \cdot \overrightarrow{\mathbf{v_1 v_3}}, \quad \text{and} \overrightarrow{\mathbf{v_2 p_2}} = \frac{\lambda - f_{appr2}(\mathbf{v_2})}{f_{appr2}(\mathbf{v_3}) - f_{\mathbf{appr2}}(\mathbf{v_2})} \cdot \overrightarrow{\mathbf{v_2 v_3}}$$

If instead property 2. is verified, then:

$$\overrightarrow{\mathbf{v_1 p_1}} = \frac{\lambda - f_{appr2}(\mathbf{v_1})}{f_{appr2}(\mathbf{v_3}) - f_{\mathbf{appr2}}(\mathbf{v_1})} \cdot \overrightarrow{\mathbf{v_1 v_3}}, \quad \text{and} \overrightarrow{\mathbf{v_1 p_2}} = \frac{\lambda - f_{appr2}(\mathbf{v_1})}{f_{appr2}(\mathbf{v_2}) - f_{\mathbf{appr2}}(\mathbf{v_1})} \cdot \overrightarrow{\mathbf{v_1 v_2}}.$$

Once we find all the possible couples $(\mathbf{p_1}, \mathbf{p_2})$, we smoothly interpolate the obtained sample of points in an *iso-geodesic* curve.

3.3 Connectivity of the graph

During the graph extraction operation, we replace each iso-geodesic curve C_i by one node N_i which is the arithmetic mean of the curve. We, hence, end up with a point cloud in 3 dimensions. In order to systematically get a final topological representation of the 3D object, we define a canonical relationship $\Re$ between every two nodes N_i and N_j such that:

$$\Re(N_i, N_j) = \begin{cases} 1 & \text{if } N_i \text{ and } N_j \text{ are connected,} \\ 0 & \text{, otherwise.} \end{cases}$$

To that end, we enounce the following postulates:

- Two nodes representing the same iso-geodesic level are disconnected. We write:

$$i = j \Longrightarrow \Re(N_i, N_j) = 0. \tag{10}$$

- Two nodes separated by nodes at intermediate levels are disconnected, *i.e.*,

$$j \neq i \pm l \Longrightarrow \Re(N_i, N_j) = 0, \tag{10}$$

  where l is the sampling step.

Based on these postulates, we constrain our search on nodes representing two different but consecutive iso-geodesic levels. Nodes representing two consecutive iso-geodesic curves are linked (connected) *iff* there is a *continuous path* φ joining the two curves and lying in Φ the section limited by the same iso-geodesic curves.

In general, a continuous path is defined as follows:

Definition: (*Continuous path*) A continuous path joining two points x, y in a metric space $\mathcal{M}$ is a mapping $\varphi : [a, b] \rightarrow \mathcal{M}$ such that $\varphi(a) = x, \varphi(b) = y$ and φ is continuous.
A path is said to lie in a set A if $\varphi(t) \in A$ for all $t \in [a, b]$.

Using the second postulate, we relate the *continuous path* joining two iso-geodesic curves to the GGF. Thus, we define our path on a domain $[i, i + l] \subset]0, 1]$ corresponding to the GGF. In the previous definition of the continuous path, we replace $[a, b]$ by [i, i+l]. Then, we define h as being the restriction of the GGF $g_n(\cdot)$ on the path $\varphi([i, i + l])$. We rewrite the connectivity condition as finding a function $h(\cdot)$ that is *continuous* and *monotone*.

3.3.1 Orthogonal curve

As a subtask, and before checking the properties of $h(\cdot)$ we need to find a continuous path φ joining two points sitting on two distinct boundaries of Φ, i.e., two iso-geodesic curves.

If a continuous path $\varphi \subset \Phi$ exists, then the shortest geodesic path has to be a continuous path. Therefore, we only need to find the shortest path linking two points on the boundaries. We herein propose a new technique for finding the shortest path that we call *orthogonal curve*.

Definition: (Orthogonal curves) An orthogonal curve on a surface S passing through a point p is the curve of minimal length who links the iso-geodesic curve containing p to another iso-geodesic curve.

This definition implies that an orthogonal curve takes a point p on a surface S and geodesically projects it on another iso-geodesic curve (Figure **??**). By considering an infinitesimal patch around a point p from S we approximate the patch to a disk D on which the iso-geodesic curve C becomes a segment passing through p. This segment represents the direction of zero variation of the GGF. We find that the projection of p on the next iso-geodesic segment $\acute{C}$ follows the perpendicular to C on p. Under the assumption that all points are uniformly distributed on the surface and since the iso-geodesic curve represents the direction of zero variation of the GGF, we prove that the orthogonal projection of p is equivalent to finding the direction e of highest variation of the GGF.
Hence, we construct an orthogonal curve by progressively tracking at a point level the direction of the highest variation of the GGF. We determine the direction e that maximizes the directional derivative of g_n at a point p.

$$e = \arg\max(Dg_n \cdot e(p)) = \arg\max(\lim_{t\to 0} \frac{g_n(p+te) - g_n(p)}{t}). \tag{11}$$

3.3.2 Illustration of nodes' connectivity

In Figure 4, we present an example (torus) in 2D of tests on nodes' connectivity. We use the orthogonal projection instead of a geodesic projection. We check the connectivity between the node $N(0.8, 1)$ representing the segment $C(0.8, 1)$ and the nodes $N(0.6, i)$, $i = 1, 2$, representing segments of the preceding levels $C(0.6, i)$. Notice that the continuous path (blue arrow) from $C(0.8, 1)$ to $C(0.6, 1)$ lies in the compact section Φ and doesn't cross any level outside the interval [0.6,0.8]. However, the path from the starting level $C(0.8, 1)$ to $C(0.6, 2)$ (arrow in green) intersects the level $C(1, 1)$. It follows that the nodes $N(0.8, 1)$ and $N(0.6, 2)$ are disconnected while $N(0.8, 1)$ and $N(0.6, 1)$ are linked by an edge.

ACKNOWLEDGMENTS

This work was fully funded by AFOSR F49620-98-1-0190 grant.

REFERENCES

1. Tangelder, J.W.H., Veltkamp, R.C. (2004). A Survey of Content Based 3D Shape Retrieval Methods. Proc. Shape Modeling International (pp. 145-156).
2. Jain, A. K., Murty, M. N., and Flynn, P. J. Data clustering: a review. ACM Computing Surveys 31, 3 (1999), 264323.
3. M. Hilaga, Y. Shinagawa, T. Kohmura, and T. L.Kunii: Topology Matching for Fully Automatic Similarity Estimation of 3D Shapes, Proc. SIGGRAPH, pp. 203-212, August 2001.
4. R. C. Staunton. An Analysis of Hexagonal Thinning Algorithms and Skeletal Shape Representation. Pattern Recognition, 29(7):11311146, 1996.
5. N.D. Cornea, M.F. Demirci, D. Silver, A. Shokoufandeh, S.J. Dickinson, and P.B. Kantor, 3D Object Retrieval using Many-to-many Matching of Curve Skeletons, Proc. IEEE International Conference on Shape Modeling and Applications, pp. 366-371, 2005.
6. Tony Tung, Francis Schmitt: The Augmented Multiresolution Reeb Graph Approach for Content-based Retrieval of 3d Shapes. International Journal of Shape Modeling 11(1): 91-120 (2005)
7. S. Baloch, H. Krim, I. Kogan, and D. Zenkov, Rotation invariant topology coding of 2D and 3D objects using Morse theory, Proc. IEEE International Conference on Image Processing, pp. 796-799, 2005.
8. Fu-Che Wu, Wan-Chun Ma, Ping-Chou Liou, Rung-Huei Laing, Ming Ouhyoung, "Skeleton Extraction of 3D Objects with Visible Repulsive Force" Computer Graphics Workshop 2003, Hua-Lien, Taiwan
9. Meng Yu; Atmosukarto, I.; Wee Kheng Leow; Zhiyong Huang; Rong Xu Computer Vision and Pattern Recognition, 2003. Proceedings. 2003 IEEE Computer Society Conference on, Vol.2, Iss., 18-20 June 2003 Pages: II- 656-61 vol.2
10. Aouada, D.; Feng, S.; Krim, H., "Statistical Analysis of the Global Geodesic Function for 3D Object Classification," Acoustics, Speech and Signal Processing, 2007. ICASSP 2007. IEEE International Conference on , vol.1, no., pp.I-645-I-648, 15-20 April 2007.
11. A. B.Hamza, and H. Krim: "Geodesic Matching of Triangulated Surfaces", IEEE transactions on image processing, Vol 15, NO. 8, pp 2249-2258, August 2006.
12. I. Grosse, P. Bernaola-Galvan, P. Carpena, R. Roman-Roldan, J. Oliver, H. Eugene Stanley: "Analysis of symbolic sequences using the Jensen-Shannon divergence", Physical Review E, Vol 65, 041905,pp 1-16, 2002.
13. A.T. Fomenco and T.L. Kunii, Topological modeling for visualization, Springer-Verlag Tokyo, 1997.

14. Y. Shinagawa, T.L. Kunii, and Y.L. Kergosien, Surface coding based on Morse theory, IEEE Comp. Graph. and Appl., vol. 11, no. 5, pp. 66-78, 1991.
15. J. Milnor, Morse theory, Princeton University Press, New Jersey, 1963.
16. X. Ni, M. Garland, and J.C. Hart, Fair morse functions for extracting the topological structure of a surface mesh, ACM Transactions on Graphics, pp. 613-622, 2004.
17. T. Lee, C. Yang, R.D. Romero and D. Mumford. Neural activity in early visual cortex reflects behavioral experience and higher-order perceptual saliency. Nature Neuroscience, Vol 5 no 6, pp 589-597, 2002.